IPST Technical Paper Series Number 549

The Lubrication Problem in a Crown-compensated Impulse Drying Press Roll

F. Bloom, B. Hojjatie, and D. Orloff

January 1995

Submitted to
Journal of Pulp and Paper Science

THE LUBRICATION PROBLEM IN A CROWN-COMPENSATED IMPULSE DRYING PRESS ROLL

F. Bloom, B. Hojjatie, and D. Orloff

We consider the lubrication problem occurring in the channel formed by the inside surface of a rotating crown-compensated impulse drying press roll and the bottom surface of an internal hydrostatic shoe. By matching the mass flow of the lubricant through the capillaries in the shoe, which feed the channel, to the mass flow in the channel itself, and using a wedge approximation to the curvilinear channel, we are able to compute, analytically, expressions for the velocity fields in each distinct subregion of the channel. From the velocity fields, and the relations describing the pressure variations in the channel, expressions are computed for all the tangential and normal forces acting on the bottom of the shoe and the inside surface of the roll; these forces are subsequently resolved into horizontal and vertical components which are then employed to set up a system of three equilibrium equations governing the balance of all horizontal and vertical forces acting on the bottom surface of the shoe as well as balance of the moments of these forces. The equilibrium equations form a system of three nonlinear coupled transcendental algebraic equations and are solved numerically, for given loads on the shoe, and tangential speeds of the roll, by an iterative procedure. A complete discussion of results for two different shoe/roll configurations is presented along with some comparisons with experimental data.

Frederick Bloom
Department of Mathematical Sciences
Northern Illinois University
DeKalb, IL 60115

Barry Hojjatie and David Orloff
Engineering and Paper Materials Division
Institute of Paper Science and Technology
500 10th St., N.W.
Atlanta, GA 30318-5794

INTRODUCTION

Energy intensive evaporative drying is currently used to dry paper but research has demonstrated that a significant savings in energy could be realized by implementing the newer impulse drying technology. In figure 1 (taken from Orloff, Jones and Phelan [1]), we show a crown-compensated (CC) extended-nip press which is configured with a ceramic coated press roll. The roll (see figure 2) revolves at high speed, counterclockwise, and is loaded, in the impulse drying mode, by the internal hydrostatic support element. Oil is injected through capillaries in the hydrostatic support element, i.e., the shoe, so as to produce an oil film (between the bottom of the shoe and the inside surface of the roll) which provides lubrication and, also, acts as a heat sink for heat lost to the interior of the roll. In the overall process, wet paper sheets transported on felt enter an extended nip at point A, in figure 1, and leave the nip at point C, while the roll itself is heated in a zone from point D to point E so as to achieve a prescribed roll surface temperature at the entrance to the nip at point A. In this paper, we consider the problem of fluid flow in the channel formed by the (curved) bottom of the internal shoe and the inside surface of the roll. It is assumed that the arcs describing the bottom of the shoe and the inside surface of the roll lie on circles of radii R_s and R, respectively, where we may have either $R_s = R$ or $R_s < R$. The actual channel, with curved walls, is approximated by a planar walled convergent channel or wedge; this planar walled channel is formed by inscribing appropriate secant lines within the circles describing the bottom of the shoe and the inside of the roll in a manner which is described below.

The internal shoe, is loaded by an external force F, measured per unit width of the shoe, so that the net load on the shoe is just F times the width w_{sh} of the shoe. The other key variables which enter the mathematical model are p_{sh} (the pressure at the top of the shoe), p_{exit} (the pressure at which the lubricating oil exits each of the two subchannels - for our purposes we take $p_{exit} = p_{atm}$, i.e., atmospheric pressure) $\tilde{R}_{eff}$ and $\tilde{l}_{eff}$ (respectively, the effective radius and length of each of the capillaries), $\Phi = 2\varphi$ (the angle subtended by those radii, in the circle describing the shoe, through the endpoints of the arc coincident with the bottom of the shoe), s (the linear speed of the inner surface of the roll), and μ and ρ (respectively, the viscosity and density of the lubricating oil). In this model it is assumed that the viscosity μ is constant.

As a consequence of the loading of the internal shoe, the pressure difference $p_{sh} - p_{exit}$, and the counterclockwise motion of the roll, the shoe will be forced downward and will deflect clockwise once the shaft of the shoe has been displaced to the right and a rib located (see figure 3) at the top of this shaft comes into contact with the confinement wall; when contact is made the shoe will also slide up and down along the confinement wall without friction.

The point $(0, R)$ in figure 3 is the location of the center of the circle describing the in-

side surface of the roll so that $(0,0)$ is the point of contact (tangency) between the roll and the paper. The center of the circle describing the bottom surface of the shoe is located at $(a, R+b)$ where a, b are determined by a set of coupled, nonlinear equilibrium equations. The points E and B lie, respectively, at the centers of the top of the shaft of the shoe and the arc describing the bottom surface of the shoe. The line segments from $(a, R+b)$ to A, B, and C are radii of the shoe of length $R_s \leq R$, while ψ is always the angle between the center line of the shoe (through E, B) and that radius of the circle describing the roll which goes through $(0, R)$ and $(0,0)$. The lubrication channel is formed by the arcs $\widehat{ABC}$ and $A'B'C'$ and a base lubrication thickness d_o may be measured along the segment $\overline{BB'}$. An approximating planar-walled channel (or wedge) is then constructed by using the secant lines through the points A, C and A', C'. The geometry which results is clearly indicated in figure 4. In the model there are two primary (independent) variables: the angle ψ and the parameter b in figure 3.

The variables ψ and b are determined by enforcing equilibria of forces in both the vertical and horizontal directions as well as balance of moments of forces acting on the internal hydrostatic shoe; the equilibrium equations depend on carefully deriving analytical expressions for all the normal and tangential forces acting on the bottom surface of the shoe (figure 4), and turn out to be a system of coupled, nonlinear, transcendental algebraic equations which can be numerically solved by an iterative procedure. Once ψ and b have been determined it is then possible to compute all the geometrical quantities which are needed in order to fix the size and shape of the approximate wedge-shaped channel, as well as the pressures $\tilde{p}_R$ and $\tilde{p}_L$ in each of the two sets of recesses, the mass flow rates $\dot{m}_R$ and $\dot{m}_L$ in each subchannel lying, respectively, to the right and left of these sets of recesses, and the explicit forms of the velocity fields in the subchannels. The velocity fields are two-dimensional and are obtained by imposing the standard lubrication theory assumption (e.g., [2],[3]) of pseudo-plane Couette flow. The expressions obtained for the tangential force exerted by the lubricating oil on the inside surface of the roll may be used to compute the net drag force acting on the roll.

Inasmuch as the equilibrium equations yield implicit relations for ψ and b of the form

$$\begin{cases} \psi = \psi(F, p_{sh} - p_{exit}, s, R, \phi, R_s, \tilde{R}_{eff}, \tilde{l}_{eff}, \mu, \rho) \\ b = b(F, p_{sh} - p_{exit}, s, R, \phi, R_s, \tilde{R}_{eff}, \tilde{l}_{eff}, \mu, \rho) \end{cases} \tag{1}$$

one may, in principle, study the effect of holding all variables in the parameter space $\mathcal{P}$

$$\mathcal{P} = \{F, p_{sh} - p_{exit}, s, R, \phi, R_s, \tilde{R}_{eff}, \tilde{l}_{eff}, \mu, \rho\} \tag{2}$$

fixed except for one, say, s, in order to study how ψ and b vary with the speed of the roll; this same procedure yields valuable information on how, e.g., the drag on the roll of

the net mass flow rate varies with s if all other elements in the parameter space $\mathcal{P}$ are frozen.

PHYSICAL MODELING OF THE LUBRICATION PROBLEM: THE EQUILIBRIUM EQUATIONS.

If we let $\bar{p}_R(x), l_\beta \leq x \leq L_\beta$, denote the pressure in the channel to the right of the right-hand recesses (figure 4) and $\bar{u}_R(x,y)$ the corresponding velocity field,

$$\bar{u}_R(x,y) = \frac{1}{2\mu}\bar{C}_R(x)y(d_R(x)-y) + s(1-yd_R^{-1}(x)), l_\beta \leq x \leq L_\beta \tag{3}$$

with $\bar{C}_R(x) = -\bar{p}_{R'}(x)$ the negative of the pressure gradient. The velocity field $\bar{u}_R(x,y)$ satisfies $\bar{u}_R(x,0) = s, \bar{u}_R(x,d_R(x)) = 0$ for all $x, l_\beta \leq x \leq L_\beta$. If we assume that $\dot{m}_R$ is independent of x one can show that

$$\bar{p}_R(x) - \tilde{p}_R = \frac{6\mu}{\tan\beta}[s(d_R^{-1}(x) - d_R^{-1}(l_\beta)) - \frac{\dot{m}_R}{\rho}(d_R^{-2}(x) - d_R^{-2}(l_\beta))] \tag{4}$$

In an analogous manner, for the left-hand subchannel (figure 4) the velocity field $\bar{u}_\mathcal{L}(x,y)$ is

$$\bar{u}_\mathcal{L}(x,y) = \frac{\bar{C}_\mathcal{L}(x)}{2\mu}y(d_\mathcal{L}(x)-y) - s(1-yd_\mathcal{L}^{-1}(x)), l_\beta \leq x \leq L_\beta \tag{5}$$

and the pressure distribution is

$$\bar{p}_\mathcal{L}(x) - \tilde{p}_\mathcal{L} = \frac{6\mu}{\tan\beta}[s(d_\mathcal{L}^{-1}(x) - d_\mathcal{L}^{-1}(l_\beta)) + \frac{\dot{m}_\mathcal{L}}{\rho}(d_\mathcal{L}^{-2}(x) - d_\mathcal{L}^{-2}(l_\beta))] \tag{6}$$

We may relate the mass flow rates per unit depth, i.e., $\dot{m}_R$ and $\dot{m}_\mathcal{L}$, to the roll speed s and the difference $p_{sh} - p_{atm}$ where $p_{atm} = p(L_\beta)$. If n_c denotes the number of capillaries which feed lubricant into each of the two subchannels, then by assuming Hagen-Poiseuille flow in the capillaries, which are idealized to be circular cylindrical tubes of length $\tilde{l}_{eff}$ and radius $\tilde{R}_{eff}$, and matching the flow through the capillaries to the flow in the two basic subchannels, we obtain the relations

$$\frac{\dot{m}_R}{\rho} = \left[(p_{sh}-p_{atm}) + \frac{6\mu s}{\tan\beta}\left(\frac{\lambda_R}{\delta_R}\right)\right] \Big/ \left[\frac{6\mu}{(\tan\beta)\delta_R} + (\frac{w_{sh}}{n_c})\frac{8\mu\tilde{l}_{eff}}{\pi\tilde{R}_{eff}^4}\right] \tag{7}$$

and

$$\frac{\dot{m}_\mathcal{L}}{\rho} = \left[(p_{sh}-p_{atm}) + \frac{6\mu s}{\tan\beta}\left(\frac{\lambda_\mathcal{L}}{\delta_\mathcal{L}}\right)\right] \Big/ \left[\left(\frac{w_{sh}}{n_c}\right)\frac{8\mu\tilde{l}_{eff}}{\pi\tilde{R}_{eff}^4} - \frac{6\mu}{(\tan\beta)\delta_\mathcal{L}}\right] \tag{8}$$

where $\lambda_R, \lambda_{\mathcal{L}}, \delta_R, \delta_{\mathcal{L}}$ are geometrical parameters defined in the nomenclature.

The normal and tangential forces exerted on both the roll and the shoe in those regions of the right and left-hand subchannels which lie, respectively, between the end of the sets of recesses in the right-hand subchannel and the end of that subchannel and between the beginning of the left-hand subchannel and the point where the set of recesses in the left-hand subchannel begin, may be computed using (3)-(6). It is easily shown, e.g., that

$$\begin{aligned}\bar{N}_{sh}^{R} &= \frac{6\mu s}{\tan^2\beta}\ln\left[\frac{d_R(L_\beta)}{d_R(l_\beta)}\right] + \frac{6\mu s}{\tan\beta}\cdot\frac{(L_\beta - l_\beta)}{d_R(l_\beta)} - \frac{6\mu}{\tan^2\beta}\left(\frac{\dot{m}_R}{\rho}\right)\left[\frac{1}{d_R(l_\beta)} - \frac{1}{d_R(L_\beta)}\right] \\ &\quad - \frac{6\mu}{\tan\beta}\left(\frac{\dot{m}_R}{\rho}\right)\frac{(L_\beta - l_\beta)}{d_R^2(l_\beta)} \qquad (9)\end{aligned}$$

$$\bar{\mathcal{T}}_{sh}^{R} = \frac{6\mu}{\tan\beta}\left(\frac{\dot{m}_R}{\rho}\right)\left[\frac{1}{d_R(L_\beta)} - \frac{1}{d_R(l_\beta)}\right] + \frac{2\mu s}{\tan\beta}\ln\left[\frac{d_R(L_\beta)}{d_R(l_\beta)}\right], \qquad (10)$$

with analogous expressions for $\bar{N}_{sh}^{\mathcal{L}}$ and $\bar{\mathcal{T}}_{sh}^{\mathcal{L}}$, while $\tilde{N}_{sh}^{R} = \tilde{p}_R \cdot w_{rec}$ yields the magnitude of the normal forcing acting on the inside surface of the recesses in the right-hand subchannel and a similar expression for $\tilde{N}_{sh}^{\mathcal{L}}$ applies. Complete details for all of these calculations may be found in [6].

To compute the normal forces and tangential acting on both the bottom surface of the shoe and the inside surface of the roll, in that region of the entire lubrication channel which lies between the two sets of recesses, we use the pressure distribution in that region, i.e.,

$$p_c(x) = \left(\frac{\tilde{p}_R - \tilde{p}_{\mathcal{L}}}{2l_c}\right)x + \left(\frac{\tilde{p}_R + \tilde{p}_{\mathcal{L}}}{2}\right), -l_c \le x \le l_c \qquad (11)$$

and the velocity field ($d(x) = d_o - x\tan\beta$)

$$u^c(x,y) = \left(\frac{\tilde{p}_{\mathcal{L}} - \tilde{p}_R}{4\mu l_c}\right)y(d(x) - y) + s(1 - yd^{-1}(x)), -l_c \le x \le l_c, \qquad (12)$$

The total normal force on that part of the bottom surface of the shoe which bounds this 'center' channel is then

$$\overset{c}{N}_{sh} = \frac{1}{2}(\tilde{p}_R - \tilde{p}_{\mathcal{L}})l_c \qquad (13)$$

while the net tangential force exerted by the lubricant on the shoe in this region is

$$\overset{c}{\mathcal{T}}_{sh} = \left(\frac{\tilde{p}_{\mathcal{L}} - \tilde{p}_R}{2}\right)d_0 + \frac{\mu s}{\tan\beta}\ln\left[\frac{d(-l_c)}{d(l_c)}\right] \qquad (14)$$

Analogous expressions are easily computed for all the normal and tangential forces exerted on the inside surface of the roll. The horsepower which must be expended to overcome the frictional force exerted on the roll by the lubricant at a given tangential speed, and a given load on the shoe, is computed using the net tangential force acting on the roll:

$$\begin{aligned}\mathcal{T}_{sl}^{net} &= \frac{6\mu}{\tan\beta}\left(\frac{\dot{m}_R}{\rho}\right)\left[\frac{1}{d_R(l_\beta)}-\frac{1}{d_R(L_\beta)}\right]+\frac{6\mu}{\tan\beta}\left(\frac{\dot{m}_{\mathcal{L}}}{\rho}\right)\left[\frac{1}{d_{\mathcal{L}}(l_\beta)}-\frac{1}{d_{\mathcal{L}}(L_\beta)}\right] \\ &+\frac{4\mu s}{\tan\beta}\left(\ln\left[\frac{d_R(l_\beta)}{d_R(L_\beta)}\right]+\ln\left[\frac{d_{\mathcal{L}}(L_\beta)}{d_{\mathcal{L}}(l_\beta)}\right]\right)+\frac{\mu s}{\tan\beta}\left(\ln\left[\frac{d_R(l_c)}{d_R(l_\beta)}\right]+\ln\left[\frac{d_{\mathcal{L}}(l_\beta)}{d_{\mathcal{L}}(l_c)}\right]\right) \\ &+\frac{1}{2l_c}(\tilde{p}_R-\tilde{p}_{\mathcal{L}})d_0 l_c+\frac{\mu s}{\tan\beta}\ln\left[\frac{d_R(-l_c)}{d_R(l_c)}\right] \qquad (15)\end{aligned}$$

If the angles $\eta_R, \eta_{\mathcal{L}}$ are now defined by

$$\tan\eta_R = \frac{\cos\psi-\cos(\varphi-\psi)}{\sin(\varphi-\psi)-\sin\psi} \qquad (16)$$

and

$$\tan\eta_{\mathcal{L}} = \frac{\cos\psi-\cos(\varphi+\psi)}{\sin(\varphi+\psi)-\sin\psi} \qquad (17)$$

then the sum of all vertical components of all forces (normal and tangential), acting on the bottom surface of the shoe can be shown to be given by

$$\begin{aligned}V_{sh} &= \bar{N}_{sh}^R\cos\eta_R+\tilde{N}_{sh}^R\cos\psi+\overset{c}{N}{}_{sh}^R\cos\eta_R+\bar{\mathcal{T}}_{sh}^R\sin\eta_R+\overset{c}{\mathcal{T}}{}_{sh}^R\sin\eta_R+\bar{N}_{sh}^{\mathcal{L}}\cos\eta_{\mathcal{L}} \\ &+\tilde{N}_{sh}^{\mathcal{L}}\cos\psi+\overset{c}{N}{}_{sh}^{\mathcal{L}}\cos\eta_{\mathcal{L}}-\bar{\mathcal{T}}_{sh}^{\mathcal{L}}\sin\eta_{\mathcal{L}}-\overset{c}{\mathcal{T}}{}_{sh}^{\mathcal{L}}\sin\eta_{\mathcal{L}} \qquad (18)\end{aligned}$$

while the sum of all the corresponding horizontal components is given by

$$\begin{aligned}H_{sh} &= -\bar{N}_{sh}^R\sin\eta_R+\tilde{N}_{sh}^R\sin\psi-\overset{c}{N}{}_{sh}^R\sin\eta_R+\bar{\mathcal{T}}_{sh}^R\cos\eta_R+\overset{c}{\mathcal{T}}{}_{sh}^R\cos\eta_R+\bar{N}_{sh}^{\mathcal{L}}\sin\eta_{\mathcal{L}} \\ &-\tilde{N}_{sh}^{\mathcal{L}}\sin\psi+\overset{c}{N}{}_{sh}^{\mathcal{L}}\sin\eta_{\mathcal{L}}+\bar{\mathcal{T}}_{sh}^{\mathcal{L}}\cos\eta_{\mathcal{L}}+\overset{c}{\mathcal{T}}{}_{sh}^{\mathcal{L}}\cos\eta_{\mathcal{L}} \qquad (19)\end{aligned}$$

In (18) a (+) sign denotes forces which act in the direction of the positive y axis, while in (19) a (+) sign denotes forces which act in the direction of the positive x-axis.

Besides the normal and tangential forces which act along the bottom surface of the shoe, there are several other forces which act on the internal hydrostatic shoe and, thus, affect its

equilibrium configurations; the major contributing forces are as follows:

(i) the load F (figure 5) applied at the top of the shaft of the shoe, which has a vertical component $V_F = -F\cos\psi$ and a horizontal component $H_F = -F\sin\psi$

(ii) the weight of the shoe W, which acts, downward at the location of the centroid (CT) of the shoe so that $V_W = -W$ and $H_W = 0$.

(iii) a horizontal reaction force H_{PV} which is exerted at the pivot point PV (figure 5).

The equations expressing equilibrium in the horizontal and vertical directions are

$$H_{sh} + H_F + H_s - H_{PV} = 0 \tag{20}$$

and

$$V_{sh} + V_F + V_W = 0 \tag{21}$$

For the equation expressing balance of moments of forces, we take moments with respect to the point B on the bottom surface of the shoe (figure 5). Denoting moments which tend to turn the shoe clockwise with a plus $(+)$ sign, and those which tend to turn the shoe counterclockwise with a minus $(-)$ sign, we find that the net moment exerted by those forces which act either inside the recesses or along the bottom surface of the shoe is given by

$$M_{sh} = \frac{1}{2}(L_{rec} + L_T)(\tilde{N}_{sh}^{\mathcal{L}} - \tilde{N}_{sh}^{R}) + d_{rec}(\tilde{N}_{sh}^{\mathcal{L}} - \tilde{N}_{sh}^{R}) + \frac{1}{2}L_c(\overset{c\,\mathcal{L}}{N}_{sh} - \overset{c\,R}{N}_{sh}) \tag{22}$$

If we set $\tilde{d} = \{$ distance between point B and the centroid CT of a cross section of the shoe$\}$ then the weight of the shoe contributes a moment equal to $M_W = W\tilde{d}\sin\psi$. As the load F applied to the shoe acts along the line through $\overline{BE}$, (figure 5) its net moment with respect to point B is zero. Finally, the moment of H_{PV} with respect to point B (figure 5) is $M_{PV} = -H_{PV}\cdot d_{PV}$; where, $d_{PV} = y_{PV} - y_B$; a precise numerical value for d_{PV} may be read off a blueprint. The complete equation expressing balance of moments of forces for the internal shoe is

$$M_{sh} + M_W + M_{PV} = 0 \tag{23}$$

The full set of equilibrium equations for the internal shoe consists of (20), (21), and (23); this system of three coupled, nonlinear, algebraic transcendental equations may easily be reduced to a system of two coupled equations by solving for H_{PV} from (20). We remark that the system (20), (21), and (23) is an algebraic system of the form

$$\begin{cases} \mathcal{G}_H(F, s, p_{sh} - p_{atm}, R, \phi, R_s, \tilde{R}_{eff}, \tilde{l}_{eff}, \mu, \rho; b, \psi) = 0 \\ \mathcal{G}_V(F, s, p_{sh} - p_{atm}, R, \phi, R_s, \tilde{R}_{eff}, \tilde{l}_{eff}, \mu, \rho; b, \psi) = 0 \\ \mathcal{G}_M(F, s, p_{sh} - p_{atm}, R, \phi, R_s, \tilde{R}_{eff}, \tilde{l}_{eff}, \mu, \rho; b, \psi) = 0 \end{cases} \tag{24}$$

which, for fixed values in the parameter space $\mathcal{P}$, serve to determine the deflection ψ and the parameter b. Once ψ and d_0 have been determined, for the same fixed values in the parameter space $\mathcal{P}$ we may compute explicit values for $\dot{m}_R, \dot{m}_{\mathcal{L}}, \tilde{p}_R, \tilde{p}_{\mathcal{L}}, \beta, d_o$, and the leading and trailing edge thicknesses $d_{\mathcal{L}}(l_\beta)$ and $d_R(l_\beta)$, respectively. We may also compute expressions for all the velocity fields in the channel as well as for all the normal and tangential forces which act along the bottom surface of the shoe, inside the recesses, and along the inside surface of the roll. From the computation of the net tangential and normal forces exerted, e.g., on the inside surface of the roll, one may readily compute both the horsepower required to overcome the frictional force exerted on the roll by the lubricant and the drag coefficient

$$c_D^{sl} = \frac{\sum \text{tangential forces on the roll}}{\sum \text{normal forces on the roll}}$$

Some typical numerical computations for two CC roll/internal shoe configurations are presented below, one in which $R \neq R_s$ and one in which $R = R_s$.

SOME NUMERICAL RESULTS FOR CC ROLLS

Computational Method

A FORTRAN computer program was developed (using the Microsoft FORTRAN compiler, version 5.1, on a 486 IBM-PC compatible microcomputer) to numerically solve the reduced system of two equations for the two unknown variables, b, and ψ. As the system of equations is highly non-linear, and strongly coupled in terms of b, ψ, and other variables, an iterative scheme was employed to obtain the solutions. A specific subroutine (DNEQNF) from the IMSL™ mathematical subroutine library, version 2.0 [4] was called by the FORTRAN program. This subroutine employs a modified Powell hybrid algorithm (a variation of the Newton's method) which uses a finite-difference approximation to the Jacobian matrix. In the finite difference method used to estimate the Jacobian, we employ double precision for all real variables, and take precautions to avoid large step size or increasing residuals. For each operating condition, appropriate initial guesses for b and ψ were introduced and the stopping criterion for iteration was taken to be that point at which the sum of the squares of the residual values corresponding to each equation was small (e.g., $< 10^{-3}$).

In the computer model, viscosity and density data for the oil were assumed to be 56 centipoise and 873 Kg/m^3, respectively, (typical of an ISO 150 mobil oil at a temperature of 57°C). These properties correspond to the lubricant employed in experiments conducted by the Beloit Corporation for the small roll/shoe configuration discussed below. Since the speed of the roll, and the load applied to the top of the shoe, are two of the most important input parameters which can be controlled by an operator, for specific design conditions, all the calculated values were obtained at a function of these two parameters. Calculations were

performed for selected outer surface roll speeds of 305–1067 m/min (1000–3500 ft/min) and load combinations of 35–1751 KN/m (200–10,000 PLI).

Results for a CC Roll with $R = 6.76"$, $R_s = 6.745"$

In this section we present some results that were obtained by using information provided by the Beloit Corporation [5]; the results are based on the dimensions for an actual shoe/roll configuration which has been used by Beloit to compile experimental data. In general the predictions of the model for the various speeds and loads that were tested are quite close in terms of absolute magnitudes to the experimental data provided by Beloit. Whatever differences exist in magnitudes may be attributed to a multitude of factors: the simplified manner in which the portion of the channel under the tapered ends of the shoe is being treated, the secant line approximations used for the arc describing the bottom surfaces of the shoe and the roll, the fact that the oil which exits the channel on the right is not skimmed off but, rather, re-enters the channel on the left, the fact that all machine dimensions, including the dimensions of both the shoe and roll radii, are accurate only to within 0.002" (thus meaning that what is an extremely critical parameter in this model, namely, the difference betwen the roll radius and the shoe radius might be off by as much as 0.004"), and the fact that all of the results presented are based on assuming a constant oil viscosity (the viscosity at the lubricant inlet temperature). Because of viscous dissipation, at higher loads and speeds the average temperature in the oil will be higher than it is at lower speeds and loads, and at any fixed speed and load the temperature in the oil varies (spatially) throughout the lubrication channel; it is also known that the actual viscosity μ of the lubricant varies strongly with temperature, with viscosity decreasing as temperature increases. It is thus somewhat misleading to use the same viscosity when, e.g., we compare the predictions of the model at a roll speed of 1000 ft/min and different loads of, say, 1000 PLI and 800 PLI, with the experimental data generated by Beloit, because the viscosity will no longer be the same number at the two different loads. In fact, because of thermal expansion of the metal in both the roll and the shoe, it is even conceivable that neither the roll radius nor the shoe radius remains constant. Some of these difficulties will be resolved once a temperature dependent viscosity has been introduced into the model. Finally, we note that the mathematical/numerical model appears to be very sensitive to changes in some measure of the relative difference $(R - R_s)/R$ where R is the roll radius and R_s is the shoe radius. The model is, also, at the same time, sensitive to some measure of the discrepancy between roll speed and load in the sense that branching of equilibrium solutions occurs and multiple solutions appear at relatively low loads and high speeds.

In figure 6 we provide a comparison between the lubricant film thicknesses (at the leading and trailing edges of the channel) as predicted by the IPST model and as measured by the Beloit Corporation for a fixed roll speed of 610 m/min and a number of different loads.

Figure 7 provides a comparison (at a roll speed of 610 m/min) of the average lubricant film thicknesses in the channel as predicted by the IPST model, on one hand, and as measured by the Beloit Corporation on the other; here average film thickness means the simple average of the leading and trailing edge thicknesses. Figure 8 compares (for a roll speed of 610 m/min) the volumetric flow rates in the channel as predicted by the IPST model and as measured by the Beloit Corporation. Finally, figure 9 compares (at roll speeds of 305 m/min and 610 m/min) the power required to operate the roll as predicted by the IPST model and as measured by the Beloit Corporation. All the predicted results referenced above are in good agreement with the corresponding experimental results, especially when one takes into account the extant shortcomings of the model as described at the beginning of this section and the types of experimental error that are present in the results measured by Beloit.

Results for a CC roll with $R_s = R = 20.005$"

Shown in figures 10-17 are some of the results of the analytical model for the case in which the roll and the shoe are machined to the same radius of 508.13 mm ($R_s = R = 20.005$ in). This shoe was subjected to loads in the range of 175-1751 KN/m (1000-10,000 PLI) and roll speeds of 305-1067 m/min (100-3500 ft/min). With only minor exceptions, the qualitative results obtained for this large shoe were similar to those for the small shoe. Shown in figures 10 and 11 are the lubricant film thicknesses vs. roll speed for a number of different loads. As shown in figure 10, for a fixed load, the lubrication film thickness at the trailing edge decreases with an increase in roll speed. This indicates that for the large shoe, as the roll speed increases, the influence of the deflection of the shoe on the thickness of the lubricant becomes relatively greater than that of its vertical motion; this was not observed in the results for the small shoe. Similar to the results for the small shoe, lubricant thickness and angle of deflection data indicate that operation of the large roll at higher loads will result in higher stability for the hydrostatic shoe with respect to variation in roll speed (figures 12 and 13).

In general, for this large shoe, subjected to a fixed load, the speed of the roll has no major effect on the lubricant flow rate (figure 14), while for the small roll at a fixed applied load, an increase in roll speed resulted in a small increase in the lubricant flow rate. Generally, the nonlinearity in the pressure distributions along each channel were less for the large shoe as compared with the small shoe. We show in figure 15, the lubricant pressure distribution along the lengths of both subchannels for each applied load and a roll speed of 610 m/min. In general, we found that the speed of the roll has only a small influence on the pressure distribution. For all the operating conditions, the pressure exerted by the lubricant on the inner surface of the roll is slightly higher at the right-hand recess as compared with the left-hand recess; the pressure distribution in these regions has a significant effect on water removal during the wet pressing of paper. Since the machine direction width of the piston

for the large shoe was chosen to be 152.2 mm (5.994"), the corresponding magnitude of the pressures applied to the top of the shoe will be in the range of 2.33-11.5 MPa (for the applied loads of 350-1751 KN/m). For the 'small' shoe/roll configuration, the predicted mechanical power required to overcome the frictional drag of the lubricant on the roll increases with applied load and roll speed, and the rate of increase was generally higher at higher applied loads and roll speeds. However, for the 'large' shoe/roll, operating at a fixed roll speed, the power was relatively insensitive to changes in applied load (figure 16). This indicates that a variation in the applied load does not change the magnitude of the net shear force which is exerted by the lubricant on the inner surface of the roll; at higher loads this corresponds to insensitivity of the angle of deflection of the shoe with respect to variations in applied loads. At any fixed load, the mechnical power required increased nonlinearly with increasing speed (figure 17).

SUMMARY OF RESULTS AND CONCLUSIONS

We have analyzed the lubrication problem which arises in modeling impulse drying employing a crown compensated roll. Numerical solutions of the equilibrium equations generated by the model were carried out for a small shoe/roll configuration in which the shoe radius is smaller than the inner roll radius, and for a large shoe/roll configuration in which the two radii are machined so as to be approximately equal. The numerical studies indicate that the model can be used effectively to study the dependence of channel thicknesses, the deflection of the shoe, mass flow rates, pressure distributions, and the power required to overcome the frictional force generated by the lubricant on the roll either on the load F (on the shoe) for a fixed tangential speed s (of the roll, where s refers to the speed of the inner surface of the roll) or on s for fixed F; the major results are as follows:

(i) For the small shoe/roll configuration, film thicknesses increase at fixed load with increasing roll speed while at a fixed speed the film thicknesses decrease with increasing load; for the large shoe/roll configuration the leading edge thicknesses increase while trailing edge thicknesses decrease with increasing speed at a fixed load and with decreasing loads at a fixed speed.

(ii) The clockwise deflection of the shoe increases with increasing speed at each fixed load and decreases as the load increases at any fixed speed.

(iii) For the small shoe/roll configuration, at a fixed load, the mass flow rate in the entire channel increases with increasing roll speed, the increase being nearly linear at both high and low loads; also at a fixed speed, the net mass flow rate increases with

increasing load. For the large roll/shoe configuration the mass flow rate is relatively insensitive to changes in speed for a fixed load but increases linearly with increasing load at fixed speeds.

(iv) For the small shoe/roll configuration, at a given applied load, the mechanical power required to operate the roll increases with roll speed, with the increases being larger and nonlinear at high loads, the same being true with increasing load at fixed speeds. But, for the large shoe/roll configuration, the power required to operate the roll is relatively insensitive to increases in load at a fixed speed, while the power increases nonlinearly with increasing speed at a fixed load.

(v) Over a wide range of applied loads and roll speeds, the pressure distribution along the inside surface of the roll, in the lubrication channel, is constant in the vicinity of each of the two respective sets of recesses, and falls off monotonically as one moves from each recess toward the end of the subchannel fed by that recess.

In view of the very prominent fashion that design parameters such as the radii of the shoe and roll and the angular opening of the shoe (as well as physical parameters such as the density and viscosity of the lubricating oil) enter into the expressions for b and ψ, the model can be used to predict, for given applied loads and roll speeds, the effect that specific design changes would have on lubricant thicknesses, pressure distributions, mass flow rates, lubricant velocity fields, etc. the mathematical model thus presents the engineer with what is anticipated to be an effective tool for optimizing specific design factors in the construction of the shoe/roll configuration in impulse drying.

Acknowledgements

The work reported here was supported by member companies of IPST and by the U.S. Department of Energy, Office of Industrial Programs, through Grant No. DE-FG02-8SCE40738. Their support is gratefully acknowledged. The authors also gratefully acknowledge extensive and useful discussions, related to this problem, with several of the staff members at Beloit Research & Development, Rockton, Illinois, especially David Lange and Paul Monroe.

NOMENCLATURE

Design Parameters

$\Phi = 2\phi$ - angular opening of the shoe

w_{sh} - width (depth) of the shoe

n_c - number of capillaries on each side of the shoe

$\tilde{l}_{eff}$ - effective length of a capillary

$\tilde{R}_{eff}$ - effective radius of a capillary

w_{rec} - width (length) of the inside of a recess

R_s, R - radiis of, respectively, the shoe and roll

L_c - distance (measured along the bottom surface of the shoe) from the midpoint on the bottom surface to the beginning of the recess

L_{rec} - distance (measured along the bottom surface of the shoe) from the midpoint on the bottom surface to the end of the recess

$L_T = R_s \cdot \varphi$

$\tilde{d}$ - distance from the centroid of a cross section of the shoe to the middle of the arc describing the bottom surface of the shoe

Geometrical Parameters

ψ - angle between the center line through the shoe and the vertical direction

$(a, R+b)$ - location of the center of the circle that the arc forming the bottom surface of the shoe lies on

d_0 - depth of the lubrication channel along the line through $(a, R+b)$ and the point at the middle of the arc forming the bottom surface of the shoe

PV - location of the pivot point for the shoe along the confinement wall

$(d_R(x) = d_0 - x\tan\beta)$ - thickness of the approximating lubrication channel (wedge) x units to the right of the middle of that channel

$(d_{\mathcal{L}}(x) = d_0 + x\tan\beta)$ - thickness of the approximating lubrication channel (wedge) x units to the left of the middle of that channel

d_{PV} - vertical distance of the pivot point PV above the point in the middle of the arc describing the surface of the shoe

$l_c = L_c\cos\beta; l_\beta = L_{rec}\cos\beta; L_\beta = L_T\cos\beta$

$d_R(l_\beta)$ - trailing edge thickness in the approximating lubrication channel (wedge)

$d_{\mathcal{L}}(l_\beta)$ - leading edge thickness in the approximating lubrication channel (wedge)

$$\lambda_R = \frac{d_R(l_\beta)d_R(L_\beta)}{d_R(l_\beta)+d_R(L_\beta)},\ \delta_R = \frac{d_R^2(l_\beta)d_R^2(L_\beta)}{d_R^2(l_\beta)-d_R^2(L_\beta)}$$

$$\lambda_{\mathcal{L}} = \frac{d_{\mathcal{L}}(l_\beta)d_{\mathcal{L}}(L_\beta)}{d_{\mathcal{L}}(l_\beta) + d_{\mathcal{L}}(L_\beta)},\ \delta_{\mathcal{L}} = \frac{d^2_{\mathcal{L}}(l_\beta)d^2_{\mathcal{L}}(L_\beta)}{d^2_{\mathcal{L}}(l_\beta) - d^2_{\mathcal{L}}(L_\beta)}$$

Physical Parameters

μ - viscosity of the lubricant (at a given temperature)

ρ - density of the lubricant (at a given temperature)

s - (tangential) speed of the inner surface of the roll

F - load applied to the top of the shaft of the shoe

$\tilde{p}_R$, $\tilde{p}_{\mathcal{L}}$ - pressures in the right- and left-hand recesses

p_{sh} - pressure exerted at the top of the shaft of the shoe

$p_{exit}(\equiv p_{atm})$ - exit pressure of the lubricant at the left- and right-hand ends of the lubrication channel

$\bar{p}_R(x)$ - pressure field in the (approximate) right-hand channel, $l_\beta \le x \le L_\beta$

$\bar{p}_{\mathcal{L}}(x)$ - pressure field in the (approximate) left-hand channel, $l_\beta \le x \le L_\beta$

$\bar{C}_R(x) = -\bar{p}'_R(x)$; $\bar{C}_{\mathcal{L}}(x) = -\bar{p}'_{\mathcal{L}}(x)$

$\bar{u}_R(x,y)$ - velocity field in the (approximate) right-hand channel, $l_\beta \le x \le L_\beta$

$\bar{u}_{\mathcal{L}}(x,y)$ - velocity field in the (approximate) left-hand channel, $l_\beta \le x \le L_\beta$

$\dot{m}_R$ - mass flow rate/unit depth in the right-hand channel

$\dot{m}_{\mathcal{L}}$ - mass flow rate/unit depth in the left-hand channel

$u^c(x,y)$ - velocity field in the lubrication channel for $-l_c \le x \le l_c$

$p_c(x)$ - pressure field in the lubrication channel for $-l_c \le x \le l_c$

$\bar{N}^R_{sh}$ - normal force exerted by the lubricant on the bottom surface of the shoe to the right of the right-hand recess

$\tilde{N}^R_{sh}$ - normal force exerted by the lubricant on the inside surface of the right-hand recess

$\overset{c}{N}_{sh}$ - normal force exerted by the lubricant on the bottom surface of the shoe between the recess

$\bar{N}^{\mathcal{L}}_{sh}$ - same as $\bar{N}^R_{sh}$, but to the left of the left-hand recess

$\tilde{N}^{\mathcal{L}}_{sh}$ - same as $\tilde{N}^R_{sh}$, but on the inside surfaces of the left-hand recess

$\bar{\mathcal{T}}^R_{sh}$ - tangential force exerted by the lubricant on the bottom surface of the shoe to the right of the right-hand recess

$\overset{cR}{\mathcal{T}}_{sh}$ - tangential force exerted by the lubricant on the bottom surface of the shoe between the middle of the shoe and the beginning of the right-hand recess

$\bar{\mathcal{T}}^{\mathcal{L}}_{sh}$ - same as $\bar{\mathcal{T}}^R_{sh}$, but to the left of the left-hand recess

V_{sh} - sum of the vertical components of all forces acting on the bottom surface of the shoe

H_{sh} - sum of the horizontal components of all forces acting on the bottom surface of the shoe

V_F, H_F - vertical and horizontal components of the load F

V_W, H_W - vertical and horizontal components of the weight W of the shoe

H_{PV} - horizontal reaction force of the confinement wall at the pivot point

M_{sh} - moment of all forces acting along the bottom surface of the shoe

M_W - moment of the weight of the shoe

M_{PV} - moment of the horizontal reaction force at the pivot point for the shoe along the wall of the confinement shaft

References

1. Orloff, D.I., Jones, G.L., and P.S. Phelan, "The Effects of Heating Mode and Internal Roll Temperature on Roll Durability and Efficiency of Impulse Drying," HTD-vol 193, Fundamentals of Heat Transfer in Porous Media, ASME 1992, 141-155.

2. Schlichting, H., *Boundary Layer Theory*, McGraw-Hill, 1960.

3. Batchelor, G.K., *An Introduction to Fluid Dynamics*, Cambridge University Press, 1990.

4. IMSL™ Math/Library, Fortran Subroutines for Mathematical Applications, version 2.0, User's Manual, Visual Numerics™, Houston, TX, 1991.

5. Beloit Corporation, Research and Development Center, Rockton, Illinois, private communication.

6. Bloom, R., Hojjatie, B., and D. Orloff, "Modeling of Fluid Flow and Heat Transfer in a Crown-Compensated Impulse Drying Press Roll I. The Lubrication Problem," submitted to the SIAM J. Appl. Math.

7. Bloom, F., Hojjatie B., and D. Orloff, "Modeling of Fluid Flow and Heat Transfer in a Crown-Compensated Impulse Drying Press Roll II. The Heat Transfer Problem," forthcoming.

FIGURES

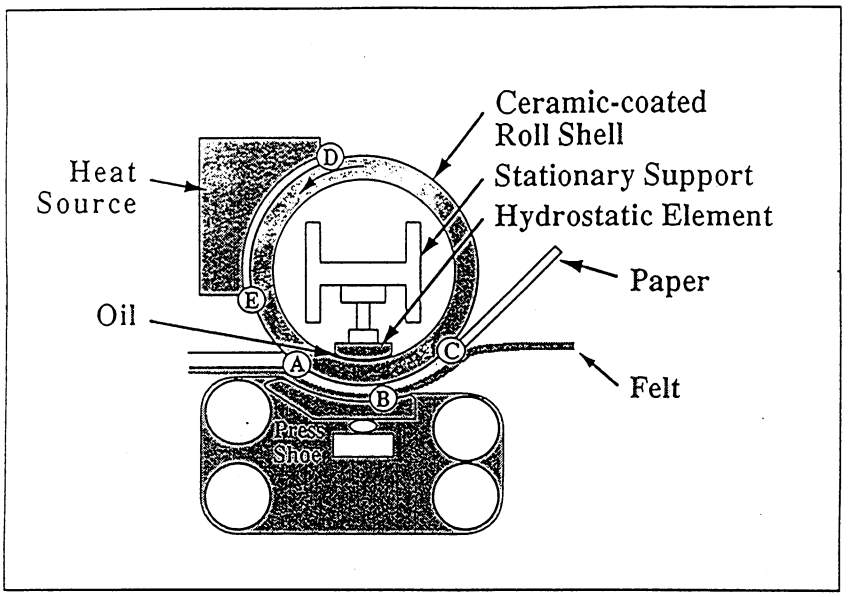

Figure 1 . The Crown Compensated Impulse Drying Press Roll (not shown to scale).

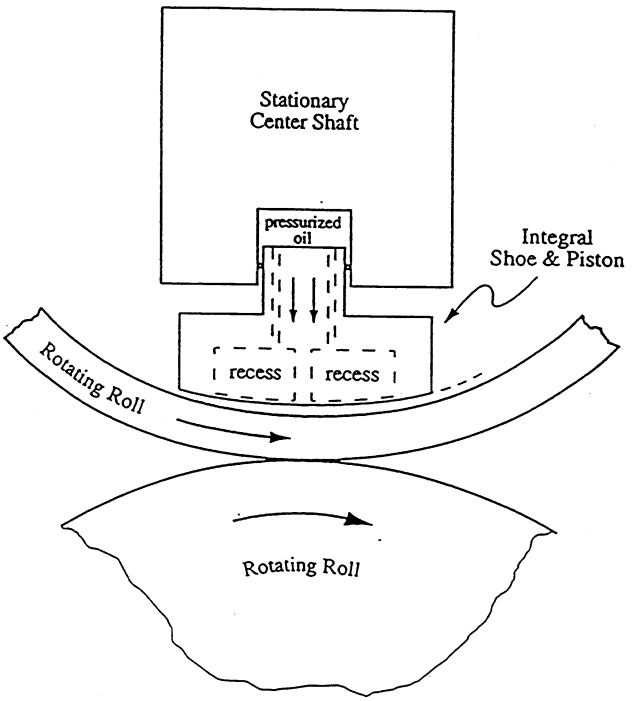

Figure 2. Cross sectional view of the shoe and the rotating shell.

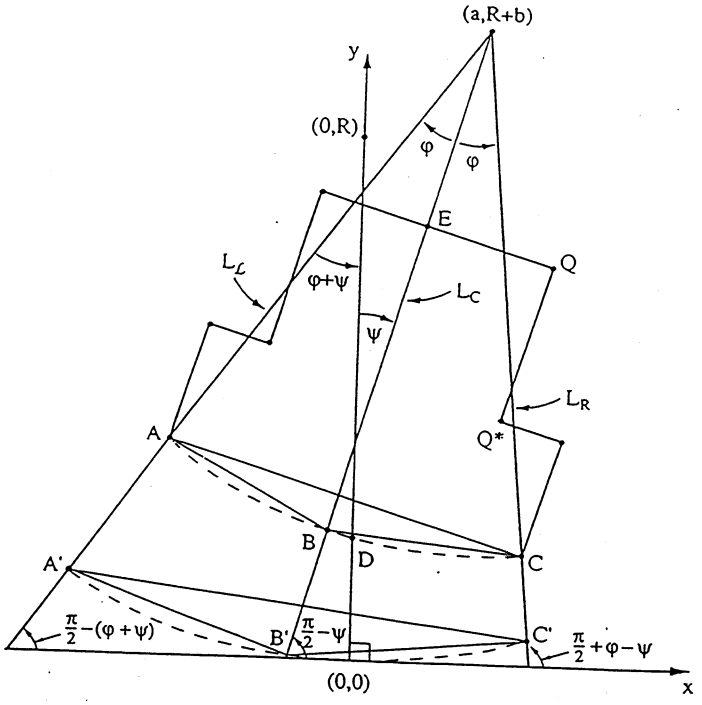

Figure 3 Motion of the hydrostatic shoe.

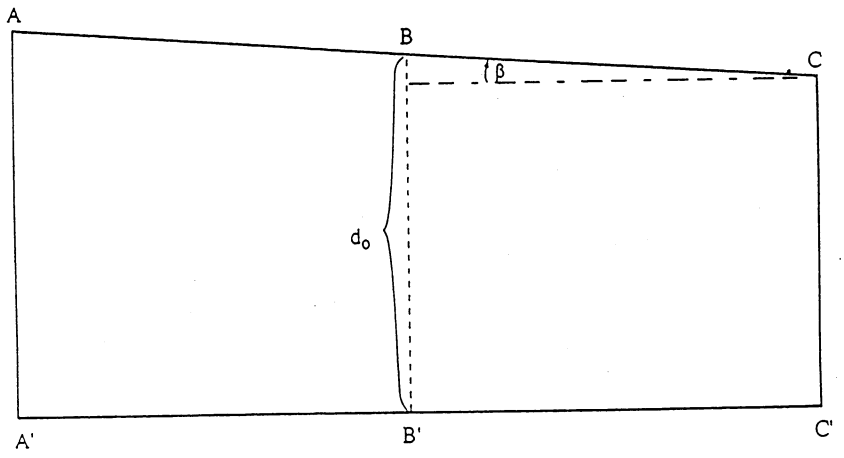

Figure 4 The approximate wedge-shaped bearing.

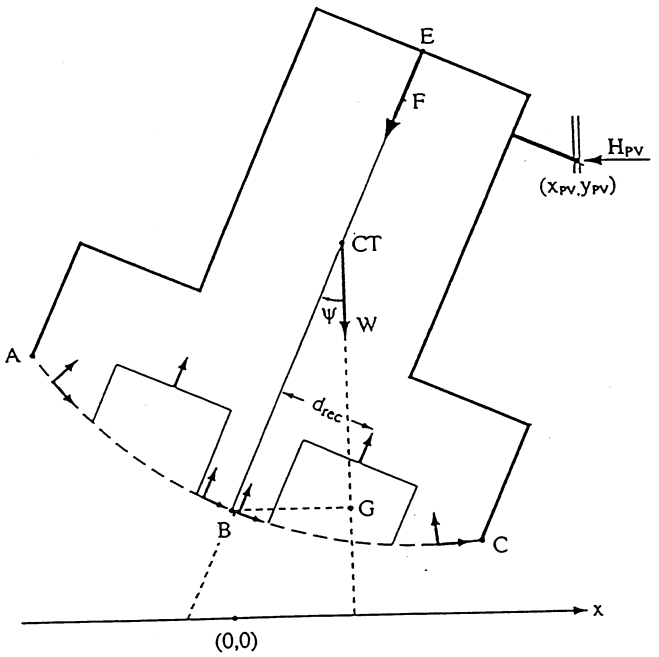

Figure 5 Forces acting on the internal hydrostatic shoe.

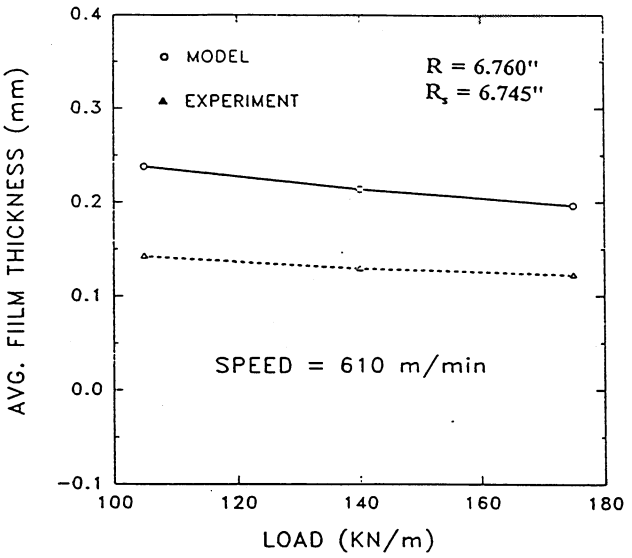

Figure 7 Comparison between the average lubricant film thicknesses (mm) predicted by the IPST model and measured by Beloit Corporation at a roll speed of 610 m/min for the roll/shoe configuration: R=6.760", R$_s$=6.745".

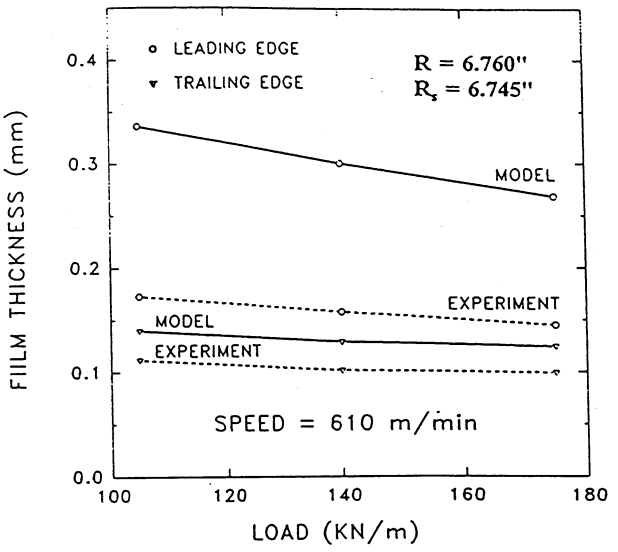

Figure 6 Comparison between the lubricant film thicknesses at the leading edge (d^L_{tp}, mm), and trailing edge (d^R_{tp}, mm) predicted by the IPST model and measured by Beloit Corporation at a roll speed of 610 m/min for the roll/shoe configuration: R=6.760", R$_s$=6.745".

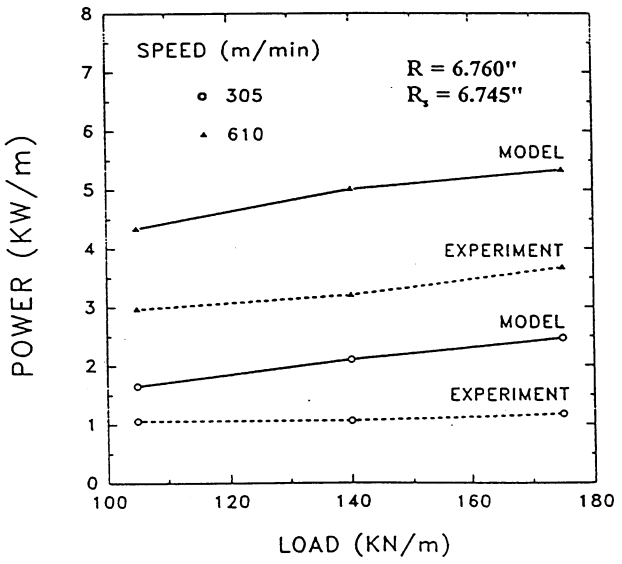

Figure 9 Comparison between the power predicted by the IPST model and measured by Beloit at roll speeds of 305 m/min and 610 m/min for the roll/shoe configuration: R=6.760", R$_s$=6.745".

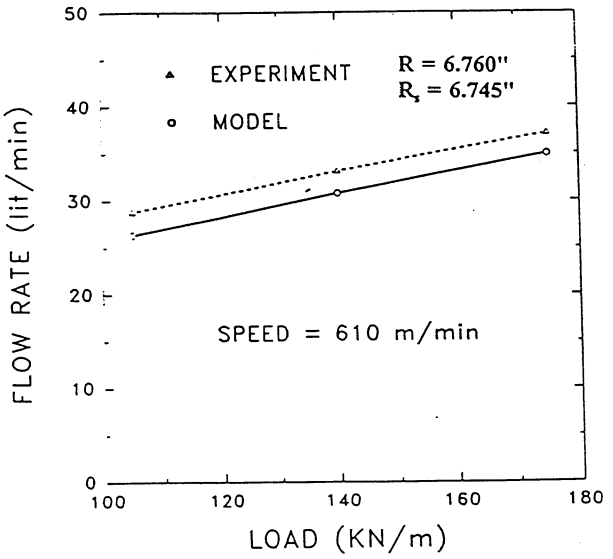

Figure 8 Comparison between the volumetric flow rate predicted by the IPST model and measured by Beloit at a roll speed of 610 m/min for the roll/shoe configuration: R=6.760", R$_s$=6.745".

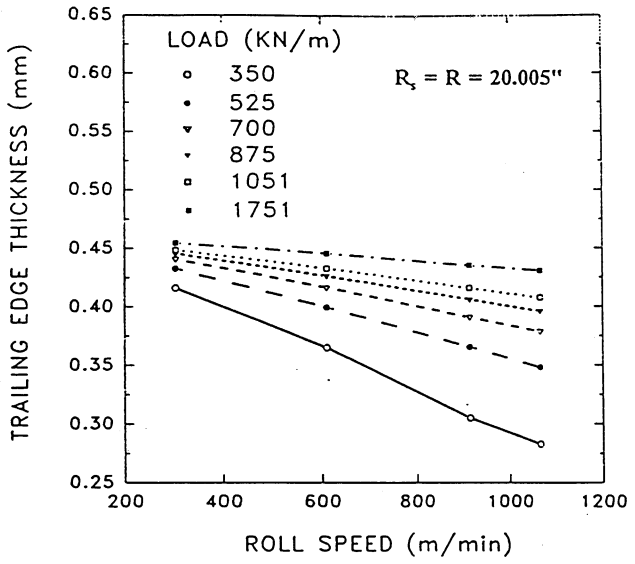

Figure 11 Lubricant film thickness at the trailing edge vs. roll speed for each applied load: R=R_s=20.005".

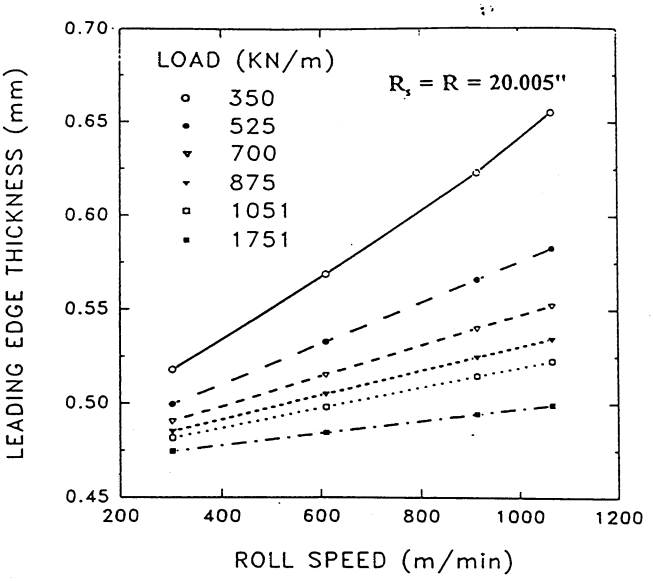

Figure 10 Lubricant film thickness at the leading edge vs. roll speed for each load applied to the "large" shoe: R=R_s=20.005".

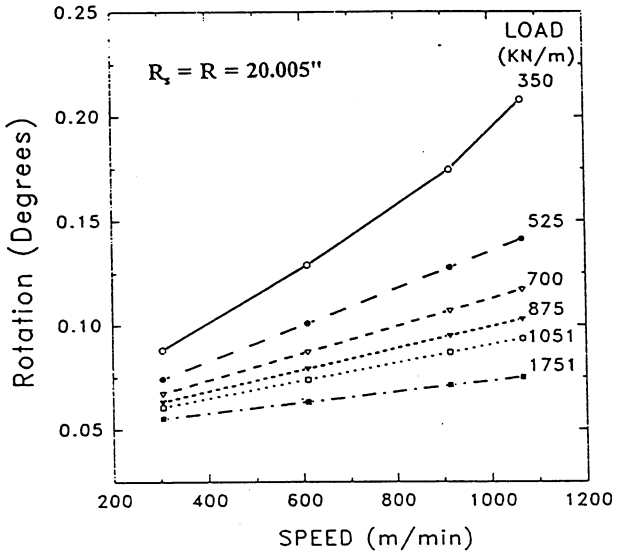

Figure 13 Angle of rotation of the shoe vs. roll speed for each applied load: R=R_s=20.005".

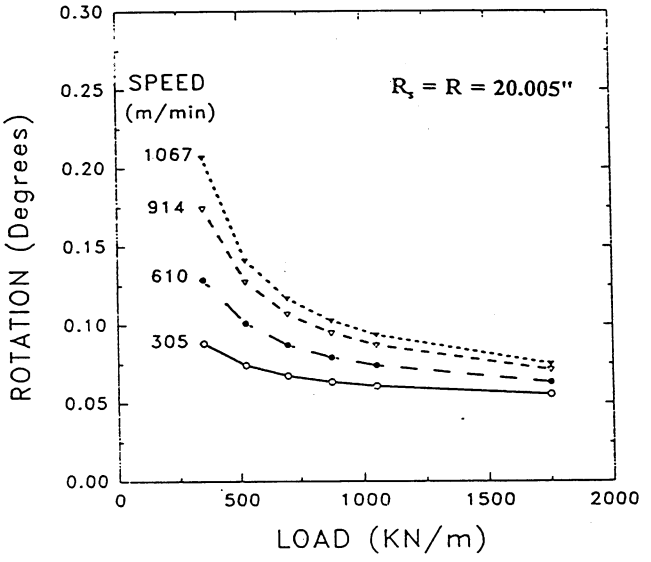

Figure 12 Angle of rotation of the shoe vs. load for each roll speed: R=R_s=20.005".

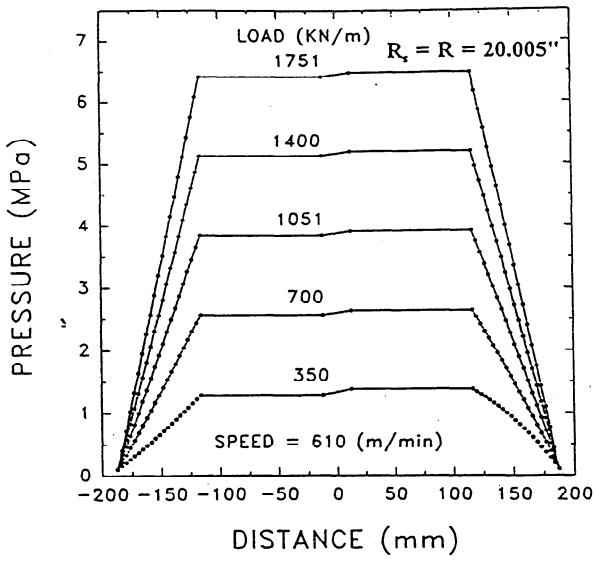

Figure 15 Lubricant pressure distribution along the length of both channels at a roll speed of 610 m/min: R=R_s=20.005".

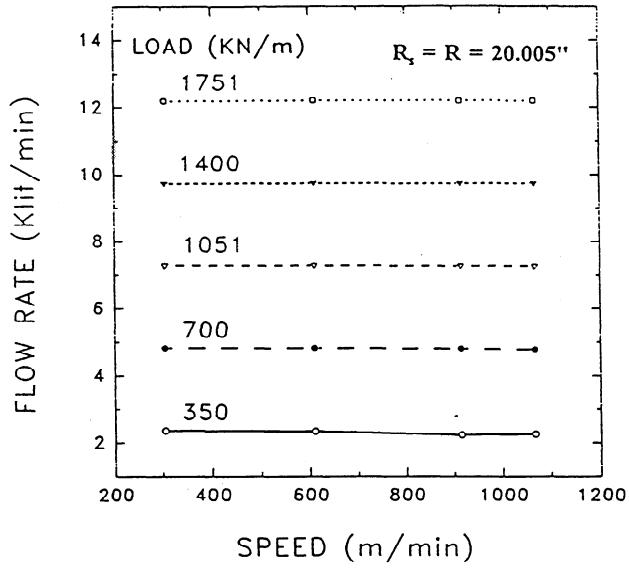

Figure 14 Lubricant total volumetric flow rate vs. roll speed for each applied load: R=R_s=20.005".

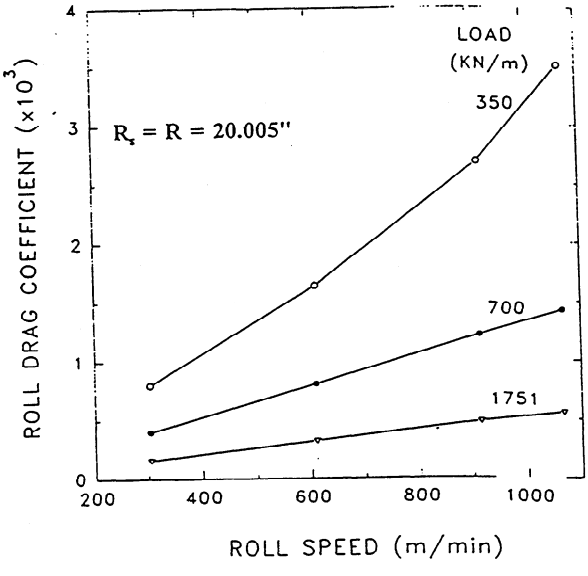

Figure 17 Roll drag coefficient vs. roll speed at each applied load: R=R_s=20.005".

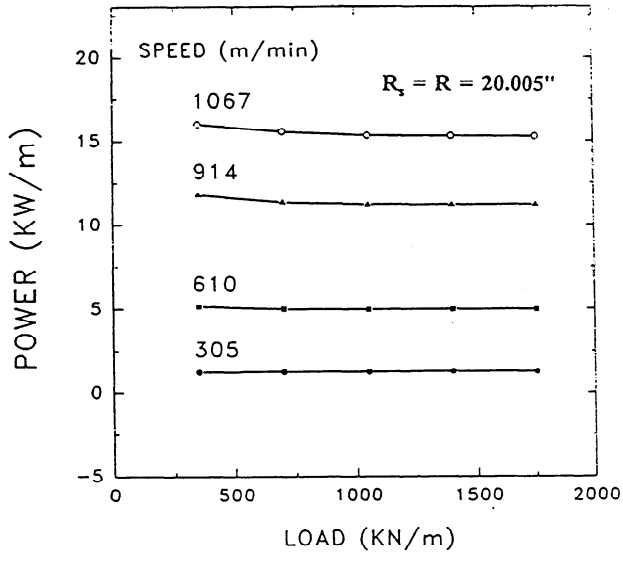

Figure 16 Mechanical power required to operate the roll vs. load for each roll speed: R=R_s=20.005".